# Near-threshold model for ultracold KRb dimers from interisotope Feshbach spectroscopy

Andrea Simoni,[1] Matteo Zaccanti,[2] Chiara D'Errico,[2] Marco Fattori,[2,3] Giacomo Roati,[2]
Massimo Inguscio,[2] and Giovanni Modugno[2]
[1]*Institut de Physique de Rennes, UMR 6251 du CNRS and Université de Rennes, 35042 Rennes Cedex, France*
[2]*LENS and Dipartimento di Fisica, Università di Firenze, and INFM-CNR, Via Nello Carrara 1, 50019 Sesto Fiorentino, Italy*
[3]*Museo Storico della Fisica e Centro Studi e Ricerche "Enrico Fermi," Compendio del Viminale, 00184 Roma, Italy*
(Received 8 February 2008; published 7 May 2008)

We investigate magnetic Feshbach resonances in two different ultracold K-Rb mixtures. Information on the $^{39}$K-$^{87}$Rb isotopic pair is combined with preexisting observations of resonance patterns for $^{40}$K-$^{87}$Rb. Interisotope resonance spectroscopy improves significantly our near-threshold model for scattering and bound-state calculations. Our analysis determines the number of bound states in singlet and triplet potentials and establishes precisely near-threshold parameters for all K-Rb pairs of interest for experiments with both atoms and molecules. In addition, the model verifies the validity of the Born-Oppenheimer approximation at the present level of accuracy.

DOI: 10.1103/PhysRevA.77.052705 PACS number(s): 34.50.−s, 03.75.−b

## I. INTRODUCTION

Magnetic Feshbach resonances [1,2] represent a unique tool for manipulating atomic quantum gases: they allow one to explore new regimes of strong interaction by modifying the collisional properties in Bose gases [3], Fermi gases [4], and mixtures [5–7]; they also enable the production of ultracold weakly bound molecules by means of magnetic-field sweeps across resonance in both homonuclear [8] and heteronuclear [9] systems. Moreover, the tight constraints set by Feshbach spectroscopy on the position of molecular energy levels closest to dissociation [10,11] can lead to a very accurate determination of long-range interaction potentials and scattering properties of the atomic system of interest.

A system that has attracted considerable interest is K-Rb: in fact, this mixture has several isotopic pairs that are easy to bring into ultracold and quantum degenerate regimes [12–15], the main isotopic combinations present several accessible Feshbach resonances [16–18], and the ground-state dimer has a relatively large electric-dipole moment [19]. Knowledge of molecular KRb potentials is crucial for studying quantitatively most phenomena in this system: on the one hand, scattering lengths and dispersion coefficients are relevant for characterizing atomic collisions and weakly bound dimers. On the other hand, the short-range potential well must be determined in order to perform experiments with deeply bound molecules. The molecular potentials of KRb have been so far constructed using different experimental inputs: Fourier transform spectroscopy and photoassociation techniques, reported most recently in Refs. [20,21], lead to a detailed knowledge of the short-range potential behavior; Feshbach spectroscopy of the $^{40}$K-$^{87}$Rb fermion-boson mixture [16–18] has allowed the long-range parameters of the system to be determined very precisely.

In this work we combine Feshbach spectroscopy on two different isotopic pairs of K-Rb and show that this significantly improves the threshold model precision. Moreover, the number of bound states supported by the interaction potentials is univocally fixed, in agreement with the recent values derived from molecular spectroscopy [21,22]. We can therefore use the model for different isotopes without being limited by typical few-bound-state uncertainties [16,23]. Finally, the availability of accurate interisotope data allows us to test possible deviations from the Born-Oppenheimer approximation.

The paper is organized as follows: Section II presents the experimental procedure used to produce an ultracold sample and to detect magnetic Feshbach resonances and zero crossings (i.e., the field locations of vanishing scattering length). Section III introduces the theoretical model and is devoted to data and error analysis; near-threshold molecular levels for selected K-Rb isotopic pairs are also presented. A brief conclusive discussion ends this work.

## II. EXPERIMENTAL METHODS

In our experimental apparatus we have investigated both the fermion-boson $^{40}$K-$^{87}$Rb and boson-boson $^{39}$K-$^{87}$Rb mixtures. With respect to the techniques for the realization and for Feshbach spectroscopy of the former mixture, we refer to [16], while we will focus here on the experimental procedure concerning the $^{39}$K-$^{87}$Rb mixture. The apparatus and techniques we used are similar to the ones we developed for the other isotopomer [16] and have already been presented elsewhere [14]. In summary, we start by preparing a mixture of $^{39}$K and $^{87}$Rb atoms in a magneto-optical trap at temperatures of the order of few 100 $\mu$K. We simultaneously load the two species in a magnetic potential in their stretched Zeeman states $|f_a=2,m_{fa}=2\rangle$ and $|f_b=2,m_{fb}=2\rangle$, and perform 25 s of selective evaporation of rubidium on the hyperfine transition at 6.834 GHz. Potassium is sympathetically cooled through interspecies collisions [15]. When the binary gas temperature is around 800 nK we transfer the mixture in an optical potential. This is created by two focused laser beams at a wavelength $\lambda=1030$ nm with beam waists of about 100 $\mu$m, crossing in the horizontal plane.

In this work we study the ground-state manifold $f_{a,b}=1$ of the $^{39}$K-$^{87}$Rb system. In general, Feshbach resonances can occur in several mixtures of Zeeman sublevels; however, not all of these are stable against spin-exchange inelastic pro-

 

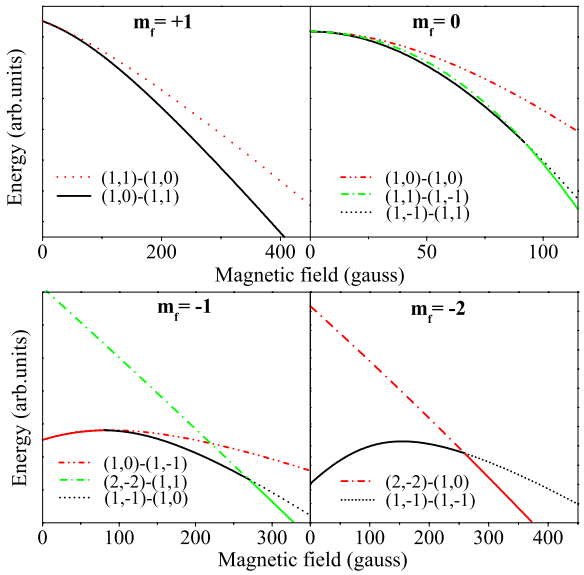


FIG. 1. (Color online) Level scheme of different $(f_a m_{fa}) + (f_b m_{fb})$ spin mixtures of $^{39}$K and $^{87}$Rb with $m_f = +1, 0, -1, -2$. For each spin combination, the solid line indicates the region where the mixture is stable against spin-exchange collisions. For each $m_f$ only the magnetic-field region where the level behavior is not trivial has been shown.

cesses. Such processes conserve the projection of the hyperfine angular momentum in the direction of the magnetic field, $m_f = m_{fa} + m_{fb}$, and the orbital angular momentum $\vec{\ell}$ of the atoms about their centers of mass. If states having internal energy lower than the initial one and the same value of $m_f$ exist, the system will in general undergo rapid spin-exchange decay.

In Fig. 1 the energies of different combinations of Zeeman states identified by the value of $m_f$ are shown and the stability region of every mixture is marked with a solid line. As convention, the first state refers to potassium and the second one to rubidium.

We have investigated the combinations $|1,1\rangle + |1,1\rangle$ and $|1,0\rangle + |1,1\rangle$, which are always stable, and $|1,-1\rangle + |1,-1\rangle$ in its stability region. The atoms are initially prepared in $|1,1\rangle$ by two consecutive adiabatic rapid passages over the hyperfine transitions around 485 MHz for $^{39}$K and 6857 MHz for $^{87}$Rb, in a 10-G homogeneous magnetic field. The transfer efficiency is typically better than 90% and the nontransferred atoms are removed by means of a few microsecond blast of resonant light. Both species are transferred from the $|1,1\rangle$ to the $|1,-1\rangle$ state by applying a radio frequency sweep about 7.6 MHz at a 10-G field. For transferring potassium atoms from the $|1,1\rangle$ to the $|1,0\rangle$ state we ramp the magnetic field up to 38.5 G, where the Zeeman splittings of potassium and rubidium already differ by some MHz, and apply a radio frequency sweep around 28.5 MHz. Once the desired mixture is prepared, we change the external magnetic field in few tens of ms and actively stabilize it to any value below 1000 G, with a short-term stability of $\sim 30$ mG and a long-term one (day to day) better than 100 mG. We calibrate the field by means of microwave and radio frequency spectroscopy on two different hyperfine transitions of Rb.

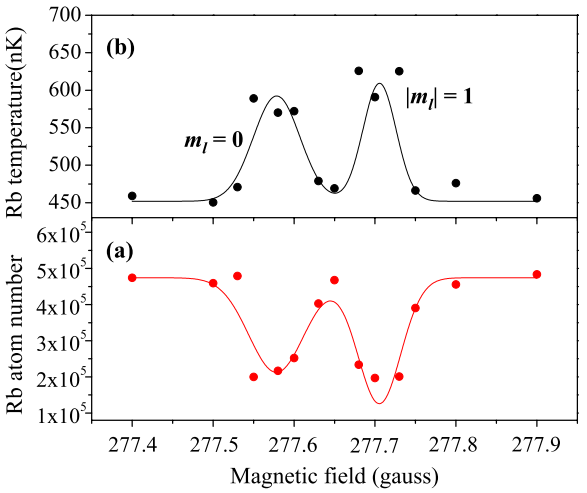


FIG. 2. (Color online) (a) Experimental Rb loss features due to a $^{39}$K-$^{87}$Rb heteronuclear $|1,1\rangle + |1,1\rangle$ $p$-wave resonance. The doublet structure is peculiar of the resonance $p$-wave character. Losses are accompanied by heating of the sample, as shown in panel (b). A similar behavior has been observed on the potassium cloud. Gaussian profiles are fitted to the experimental data in order to extract the resonance centers. The $|m_l|$ assignment of the two features is derived from a global fit of all the resonances (see text).

Heteronuclear Feshbach resonances are detected as an enhancement of three-body losses. In fact, the $s$-wave scattering length in the vicinity of a resonance varies according to the dispersive behavior

$$a(B) = a_{\mathrm{bg}}\left(1 - \frac{\Delta}{B - B_0}\right), \tag{1}$$

where $a_{\mathrm{bg}}$ is the background scattering length and $\Delta$ is the width of the resonance, defined as the distance between the

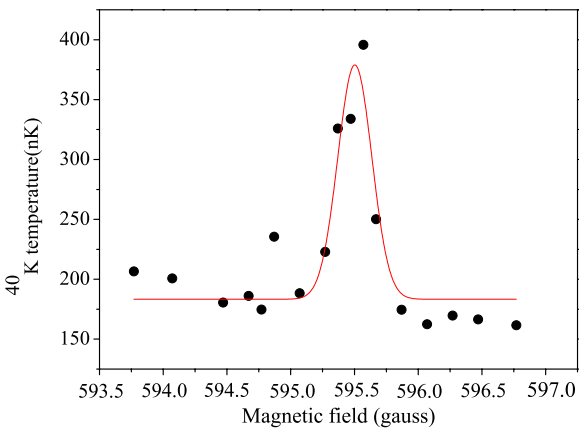


FIG. 3. (Color online) Experimental observation of the zero crossing near the 598.4-G fermion-boson resonance. As the magnetic field assumes values close to the zero-crossing point, the heterouclear elastic cross section vanishes and the efficiency of sympathetic cooling during further evaporation in the optical trap decreases. A similar behavior has been observed in the boson-boson mixture for the zero crossing associated with the resonance located at 318 G; see Table I.

TABLE I. Experimentally observed magnetic-field positions $B_{expt}$ and theoretically calculated positions $B_{th}$ for collisions of $^{39}$K and $^{87}$Rb. Few experimental zero-crossing positions have also been used for modeling and are identified with an asterisk (*). Zeeman states of the atomic fragments correlate in zero field with $|f_a m_{fa}\rangle$ and $|f_b m_{fb}\rangle$, respectively (first column). Calculations use parameters of Eq. (3). Errors shown in parentheses represent one standard deviation for both experimental and theoretical values. The magnetic widths $\Delta$ are provided for the observed $s$-wave features. In view of possible experiments of molecule formation the background scattering length $a_{bg}$ and magnetic moment $s$ are also given for resonances in the lowest Zeeman sublevel. The $\ell$ quantum number is the orbital angular momentum of the molecule associated with each resonance. The magnitude $|m|$ of its projection on the magnetic field is shown for the $\ell=1$ doublet features that have been experimentally resolved. The last column shows the spin-coupling scheme of the Feshbach molecule $\{tf_b f\}$; see text.

| $\|f_a m_{fa}\rangle+\|f_b m_{fb}\rangle$ | $B_{expt}$ (G) | $B_{th}$ (G) | $\Delta_{th}$ (G) | $a_{bg}$ ($a_0$) | $-s(\mu_B)$ | $\ell(\|m\|)$ | Assignment |
|---|---|---|---|---|---|---|---|
| $\|1,1\rangle+\|1,1\rangle$ | 247.9(2) | 248.05(3) | 0.28 | 34 | 2.8 | 0 | $\{\frac{5}{2}23\}$ |
| | 277.57(5) | 277.53(3) | | | | 1(0) | |
| | 277.70(5) | 277.70(3) | | | | 1(1) | |
| | 317.9(5) | 318.30(3) | 7.6 | 34 | 2.0 | 0 | $\{\frac{5}{2}22\}$ |
| | 325.4(5)* | 325.92(3)* | | | | 0 | |
| | 495.19(6) | 495.19(3) | | | | 1(0) | |
| | 495.62(6) | 495.65(3) | | | | 1(1) | |
| | 531.2(3) | 530.72(3) | 2.5 | 35 | 2.0 | 0 | $\{\frac{3}{2}13\}$ |
| | 616.06(10) | 615.85(4) | 9.5[−2] | 35 | 1.9 | 0 | $\{\sim\frac{3}{2}12\}$ |
| $\|1,0\rangle+\|1,1\rangle$ | 623.47(6) | 623.48(5) | 6[−3] | | | 0 | |
| | 673.62(8) | 673.76(4) | 0.25 | | | 0 | |
| $\|1,-1\rangle+\|1,-1\rangle$ | 117.6(4) | 117.59(3) | −1.3 | | | 0 | |

zero crossing and the resonance center $B_0$. As the scattering length $a(B)$ diverges, three-body inelastic rates are enhanced [24], resulting in atom loss from the trap and heating.

We have at first searched several of the broadest resonances theoretically predicted by the model of Ref. [16], which employed, however, a number of singlet bound states two units smaller than the correct one (see below); experimentally, all of them were found within a few gauss from the predicted positions. In general, the experimental location of broader resonances is affected by larger uncertainties: consequently, narrow features are crucial to improve the model precision as their position can be determined with high accuracy. For an accurate detection of such weak features, such as, for example, the resonances near 248 G in the $|1,1\rangle+|1,1\rangle$ mixture or the one at 674 G in $|1,0\rangle+|1,1\rangle$ collisions (see Table I), we have performed further studies at lower temperatures (250–350 nK) and higher densities.

Obtaining such conditions is crucial in particular for revealing $p$-wave resonances, whose complex structure [25] can be easily masked by thermal effects. The mixture is cooled by reducing the trap depth in 2.4 s with an exponential ramp. The optical potential is designed in such a way to force evaporation of rubidium along the vertical direction, while potassium is sympathetically cooled without significant atom losses. As already remarked for $p$-wave scattering between fermions [25] and more recently in a $^{40}$K-$^{87}$Rb fermion-boson mixture [7], a doublet splitting represents direct evidence of the $p$-wave character of such resonances: this feature arises from spin-spin and second-order spin-orbit interactions, as we will discuss later. The typical doublet structure has been observed for two $p$-wave resonances at 277.5 G (see Fig. 2) and 495.5 G.

The location of the zero crossing associated with broad Feshbach resonances has been determined in both fermion-boson and boson-boson mixtures by recording the efficiency of the sympathetic cooling of potassium as a function of the magnetic field applied during the evaporation in the optical potential; see [6]. In fact, in the ultracold regime the total elastic cross section vanishes with the $s$-wave scattering length resulting in a strongly reduced sympathetic cooling rate. For this kind of analysis we lower the beam intensities of the optical trap, and after 2.4 s of forced evaporation we measure the temperature of the potassium cloud as a function of the external magnetic field. As shown in Fig. 3, the position of the zero crossing appears then as a sharp peak in the potassium temperature.

The magnetic-field position of all observed Feshbach resonances is reported in Tables I and II. We also report zero-crossing positions for a few broad resonances and the doublet splitting of $p$-wave resonances for the boson-boson mixture. Thirteen of the boson-fermion features are from Ref. [16].

## III. THEORETICAL ANALYSIS

The main features of our theoretical model have already been described in Ref. [16]. At variance with our previous work we adopt here the spectroscopic singlet $^1\Sigma^+$ potential of Amiot and Vergès [26]. This potential supports the correct number $N_S^b(40-87)=100$ of rotationless vibrational levels (see below) whereas the formerly used *ab initio* potential energy curve of Rousseau *et al.* [27] only has 98. This difference is immaterial as far as one is concerned with the

TABLE II. Same as Table I, but for collisions of $^{40}$K and $^{87}$Rb. As in Table I, few experimental zero-crossing positions have been used for theoretical modeling and are identified by an asterisk (*). Note that the quantity $-\Delta_{th}$ is reported here. The last column shows the spin-coupling scheme of the Feshbach molecule $(f_a f_b f)$; see text.

| $\|f_a m_{fa}\rangle+\|f_b m_{fb}\rangle$ | $B_{expt}$ (G) | $B_{th}$ (G) | $-\Delta_{th}$ (G) | $(a_0)$ $a_{bg}$ | $-s(\mu_B)$ | $\ell$ | Assignment |
|---|---|---|---|---|---|---|---|
| $\|9/2,-9/2\rangle+\|1,1\rangle$ | 456.1(2) | 456.31(7) | | | | 1 | |
| | 495.6(5) | 495.31(12) | 0.15 | −177 | 2.7 | 0 | $(\frac{7}{2}1\frac{7}{2})$ |
| | 515.7(5) | 515.35(7) | | | | 1 | |
| | 543.3(5)* | 543.66(8)* | | | | 0 | |
| | 546.6(2) | 546.75(6) | 3.1 | −189 | 2.3 | 0 | $(\frac{7}{2}1\frac{9}{2})$ |
| | 658.9(6) | 659.02(13) | 0.80 | −196 | 2.8 | 0 | $(\frac{7}{2}2\frac{11}{2})$ |
| | 663.7(2) | 663.80(10) | | | | 2 | |
| $\|9/2,-7/2\rangle+\|1,1\rangle$ | 469.2(4) | 469.03(13) | 0.28 | | | 0 | |
| | 584.0(10) | 584.01(11) | 0.70 | | | 0 | |
| | 591.0(3) | 590.85(7) | | | | 2 | |
| | 595.5(5)* | 595.60(7)* | | | | 0 | |
| | 598.4(2) | 598.17(6) | 2.53 | | | 0 | |
| | 697.3(3) | 697.37(9) | 0.15 | | | 0 | |
| | 705.0(14) | 704.33(13) | 0.82 | | | 0 | |
| $\|9/2,-9/2\rangle+\|1,0\rangle$ | 542.5(5)* | 542.79(5)* | | | | 0 | |
| | 545.9(2) | 545.95(7) | 3.2 | | | 0 | |
| | 957.6(5)* | 957.70(13)* | | | | 0 | |
| | 962.1(2) | 962.04(13) | 4.3 | | | 0 | |
| $\|9/2,7/2\rangle+\|1,1\rangle$ | 299.1(3) | 298.51(5) | 0.61 | | | 0 | |
| | 852.4(8) | 851.93(14) | 6.1[−2] | | | 0 | |

study of a single isotope, but it would be responsible for systematic errors when the properties of other pairs are calculated.

The singlet potential energy curve is obtained at regular internuclear distances using the near-dissociation coefficients of [26] and the RKR1 code [28]. The triplet *ab initio* potential $^3\Sigma^+$ of Rousseau *et al.* provides the correct number $N_T^b(40-87)=32$ of rotationless vibrational levels (see below) and is retained for our analysis. We have now sufficient experimental information to determine both leading long-range coefficients $C_6$ and $C_8$ independently of *ab initio* calculations. The model is also parametrized in terms of *s*-wave singlet-triplet scattering lengths $a_{S,T}$ of the fermion-boson mixed system and includes relativistic spin-spin and second-order spin order corrections [29].

Our data set comprises resonances observed in two isotopic mixtures. The $^{40}$K-$^{87}$Rb fermion-boson system is now well characterized and theoretically understood [16,18]. For the $^{39}$K-$^{87}$Rb boson-boson pair, the former theoretical predictions of Ref. [16] is in good agreement with the present observations. This circumstance is in itself sufficient to conclude that $N_T^b=32$ is correct, as a $\pm 1$ variation in $N_T^b$ gives rise to shifts of $^{39}$K-$^{87}$Rb Feshbach resonances as large as 10 G, for fixed values of $a_{S,T}(40-87)$.

Shifts are in general less dramatic upon variation of the dissociation energy of the deeper $^1\Sigma^+$ potential. In addition, the boson-boson resonances observed here have mostly triplet character. Fortunately the specific feature at ~616 G has sufficient singlet mixing for its position to shift of about $\pm 3$ G per bound state added or subtracted from the $^1\Sigma^+$. This is sufficient to fix conclusively $N_S^b=100$. Our present values of $N_{S,T}^b$ confirm recent spectroscopic [21] and *ab initio* potentials [30]. After this preliminary characterization of the interaction potentials, we proceed to fine-tune the potential shape in order to reproduce the present experimental spectra. The presence of narrow resonances in our data is crucial to improve the precision of the parameters, as their position can be determined experimentally more accurately [31].

It has been recently remarked in Ref. [21] that the splitting observed in the $^{40}$K-$^{87}$Rb mixture [7] between $\ell=1$ resonances with different projections $m=0$ and $|m|=1$ of $\vec{\ell}$ along the magnetic field cannot be accounted for by electron spin-spin interactions only. Comparison of two $\ell=1$ doublet features of the boson-boson system (see Table II and Fig. 2) with theoretical calculations confirms this observation. In particular, the spin-spin induced splitting of the doublet at 495 G is found theoretically to be ~900 mG versus an observed value of ~500 mG. Within the present resolution this discrepancy might be sufficient to bias our analysis. Hence, we perform a preliminary $\chi^2$ minimization only based on *s*-wave resonances, which are virtually unaffected by spin interactions. Next, we introduce a phenomenological second-order spin-orbit operator of the form [29]

$$V_{so}(R)=\frac{C\alpha^2}{2}e^{-\beta(R-R_S)}(3S_z^2-S^2), \tag{2}$$

where $\alpha$ is the fine-structure constant, $S$ is the total electrons spin, and $z$ is taken along the internuclear axis. We assign to

the parameters $\beta$ and $R_S$ the arbitrary yet reasonable values $0.085a_0^{-1}$ and $10a_0$ whereas the strength $C$ is fixed to $1.910^{-3}E_h$ in order to reproduce the observed doublet separations. We perform a final optimization including all $\ell>0$ features for both isotopes. Result of the fit is

$$a_S(40-87) = -110.6(4)a_0,$$

$$a_T(40-87) = -214.0(4)a_0,$$

$$C_6 = 4290(2)a_0^6E_h,$$

$$C_8 = 4.79(4)\times 10^5 a_0^8 E_h. \quad (3)$$

The reduced $\chi^2$ (i.e., the $\chi^2$ per degree of freedom) is $\tilde{\chi}^2=0.84$ and the maximum discrepancy with the empirical data is less than two standard deviations. Note that the positions of $\ell=2$ features, which are also shifted by spin interactions, are well reproduced, thus confirming the quality of our analysis. Our $a_{S,T}$ fully agree with the determination of Ref. [16]. The van der Waals coefficient $C_6$ is consistent to about one standard deviation with the value $4274(13)a_0^6E_h$ given by Derevianko *et al.* [32] while $C_8$ deviates by two standard deviations from the result $4.93(6)a_0^8E_h$ of Ref. [33].

The detailed shape of the potential well usually gives unimportant corrections to cold collision observables to the extent that the scattering lengths and the long-range parameters (3) are kept fixed; see [34]. However, sample calculations with modified inner potentials show that to the current level of precision such corrections are not fully negligible and could be approximately accounted for by multiplying by an extra factor of 2 the standard deviations in Eq. (3). With this proviso, in the following we provide error bars as obtained from our current model that is thereby supposed to give a sufficiently accurate description of the short-range dynamics.

One should note that the potential parameters are statistically correlated. For instance, if $C_6$ and $C_8$ were kept constant, the position of a given experimental feature could be approximately obtained by increasing $a_S$ (i.e., by making $^1\Sigma$ *less* binding) and concurrently decreasing $a_T$ (i.e., by making $^3\Sigma$ *more* binding).

As all parameters are left to vary, correlations become more complex and can be summarized for a linearized model in the symmetric covariance matrix

$$\mathcal{C}\ \text{(a.u.)} = \begin{pmatrix} 0.14 & 2.4[-2] & -0.47 & -9.2[2] \\ \cdots & 0.18 & -0.10 & 8.3[2] \\ \cdots & \cdots & 2.1 & 4.5[3] \\ \cdots & \cdots & \cdots & 1.6[7] \end{pmatrix}. \quad (4)$$

The $\mathcal{C}$ matrix has been used to compute error bars on the theoretical resonance positions (second column in Tables I and II) using standard error propagation whereas neglect of correlations might lead to grossly overestimated uncertainties.

Our improved model is now used to determine the evolution of molecular levels near dissociation, taking advantage of the profound relation between near-threshold bound states and scattering properties; see, e.g., [34]. We first focus on the boson-boson system for the experimentally relevant case of $\ell=0$ molecules that can be magnetically associated starting from atoms in the lowest Zeeman sublevel $|11\rangle+|11\rangle$.

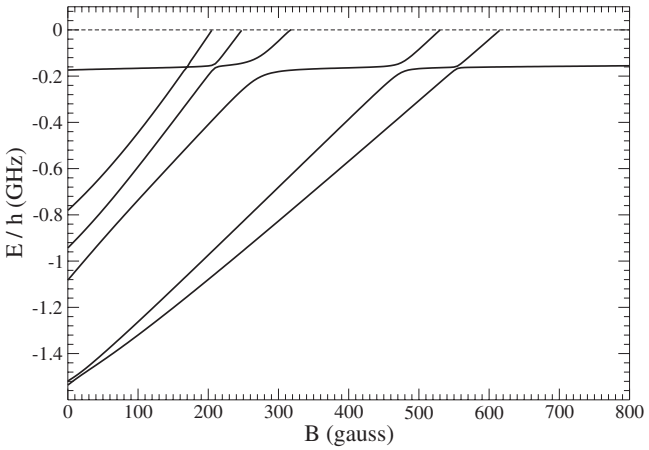


FIG. 4. Near-threshold $^{39}K^{87}Rb$, $\ell=0$, molecular levels magnetically coupled to atoms in the lowest hyperfine Zeeman sublevel. The energy of the latter is taken as zero (dashed line). Potential parameters are from Eq. (3).

Levels closest to dissociation are usually strongly affected by hyperfine interactions. This is especially the case when $a_S$ and $a_T$ have similar values since the splitting between singlet and triplet vibrational levels is then small and the corresponding quantum states are efficiently mixed by hyperfine couplings. Focusing on weak magnetic fields, in this situation the diatomic is characterized by Hund's case (e) quantum numbers $(f_a,f_b,f)$ where the total hyperfine spin vector $\vec{f}=\vec{f}_a+\vec{f}_b$ is nearly exactly conserved. As levels become more strongly bound, the spin-exchange interaction first causes decoupling of electron $\vec{s}_a$ and nuclear $\vec{i}_a$ spin on the atom which has a smaller hyperfine coupling, potassium in the present case. The hyperfine angular momentum of rubidium $\vec{f}_b$ then recouples with $\vec{s}_a$ because of spin-exchange forces to form a new vector quantity which we denote here as $\vec{t}=\vec{s}_a+\vec{f}_b$. Finally, the relatively weak potassium hyperfine interaction forces $\vec{t}$ and $\vec{i}_a$ to form the total hyperfine angular momentum $\vec{f}=\vec{t}+\vec{i}_a$. In this situation, the molecule is represented by $\{tf_bf\}$ quantum numbers. Note that we have associated different brackets with different Hund's cases in order to help to identify them.

Molecular levels for $\ell=0$ molecules in the boson-boson system are presented in Fig. 4. The bound level at −0.2 GHz running parallel to the energy of the separated atoms is associated to background scattering. That is, its position would correspond to single channel scattering with the same background scattering length and long-range coefficients. This is the only level characterized by Hund's case (e) quantum numbers (1,1,2). The five levels below, four of which experimentally observed as resonances, are all described by the intermediate $\{tf_bf\}$ quantum numbers; see Table I. One should note that near a resonance the molecular closed-state channel mixes with the open-background channel [35]. The size of the region where this happens can be estimated as [35]

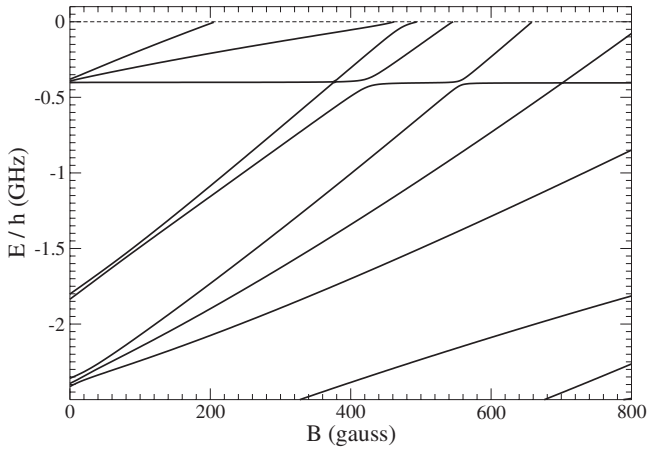


FIG. 5. Same as Fig. 4, but for $^{40}$K$^{87}$Rb.

$$\frac{B - B_0}{\Delta} \ll \frac{2\mu a_{\rm bg}^2 s\Delta}{2\hbar^2}, \tag{5}$$

where $\mu$ is the reduced mass and

$$s = -\frac{\partial E}{\partial B} \tag{6}$$

is the magnetic moment of the molecule relative to that of the separated atoms. Using the parameters in Table I one can easily check that $^{39}$K-$^{87}$Rb resonances are essentially closed-channel dominated as according to Eq. (5) mixing with the open channel is small over most of the magnetic width $\Delta$. In this situation, near-resonance effective models should involve at least on two channels characterized by the parameters of Table I; see [35].

We now discuss the fermion-boson system. As the hyperfine splitting of $^{40}$K is larger than the one of $^{39}$K and $a_S$ and $a_T$ have in this case similar values, all resonances reported in Table II belong to Hund's case (e). That is, the exchange interaction is not strong enough to decouple nuclear and electron spin of either atom. Molecular levels for the fermion-boson system are shown in Fig. 5; see also Ref. [18] for similar results. Approximate values of quantum numbers are found in Table II. Finally, using the parameters of Table II and Eq. (5) one finds that fermion-boson resonances range from closed-channel dominated to an intermediate situation, in which closed and open channels are mixed over a significant fraction of the magnetic width.

So far, in our procedure, we have used the same interatomic potential for the two isotopes thus assuming validity of the Born-Oppenheimer approximation. In order to quantify possible breakdown effects [36] we fit our data by varying *independently* the short-range potential for the two isotopes. The result of the fit is then

$$a_S(40-87) = -110.8a_0,$$

$$a_T(40-87) = -213.8a_0,$$

$$a_S(39-87) = 1.9810^3 a_0,$$

$$a_T(39-87) = 35.6a_0,$$

$$C_6 = 4291a_0^6 E_h,$$

$$C_8 = 4.80 \times 10^5 a_0^8 E_h,$$

corresponding to $\chi^2$=0.93, a slightly larger value than the one found above due to the diminished number of degrees of freedom. Note that these best-fit parameters are fully consistent with the values obtained assuming mass scaling.

We also remark that theoretical resonance positions do not show any preferential positive or negative shift with respect to the experimental ones. We can conclude that even at the present level of precision no evidence is found for a breakdown of the Born-Oppenheimer approximation. Mass scaling can then be used for predicting the properties of other isotopes. In particular, the $a_{S,T}$ along with the long-range coefficients determined in this work are sufficient in order to predict all relevant threshold properties of any K-Rb pair.

The *s*-wave singlet and triplet scattering lengths are shown in Table III for all isotopic combinations. Both $a_S$ and $a_T$ are consistent with our previous determination [16] if one corrects for the different number of bound states supported by the singlet potential, as specified in that work. Our values

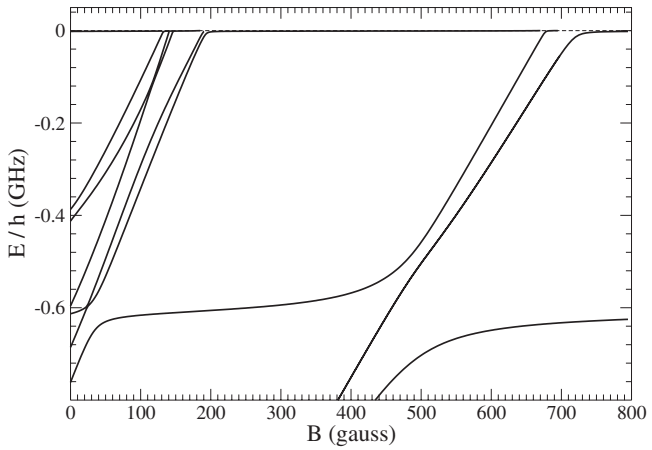


FIG. 6. Same as Fig. 4, but for $^{41}$K$^{85}$Rb.

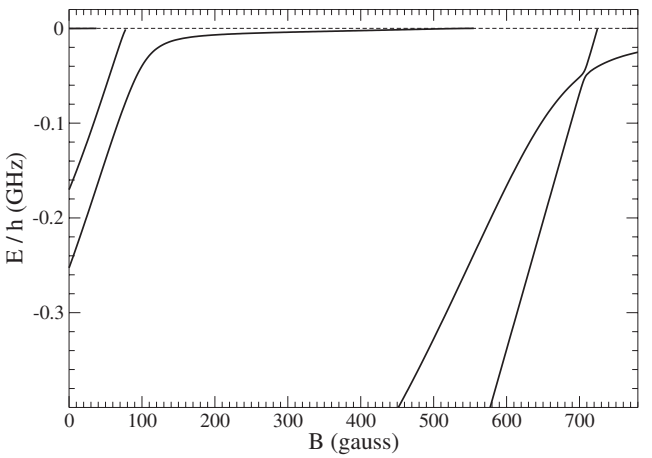


FIG. 7. Same as Fig. 4, but for $^{41}$K$^{87}$Rb.

TABLE III. Singlet and triplet *s*-wave scattering lengths for collisions between K and Rb isotopic pairs based on our spectroscopic data for both the fermion-boson and the boson-boson mixtures.

| K-Rb pair | $a_S(a_0)$ | $a_T(a_0)$ |
|---|---|---|
| 39–85 | 33.78(6) | 63.27(2) |
| 39–87 | 1.98(4)10$^3$ | 35.61(3) |
| 40–85 | 65.39(5) | −28.63(6) |
| 40–87 | −110.6(4) | −214.0(4) |
| 41–85 | 103.25(6) | 349.0(4) |
| 41–87 | 7.13(9) | 163.82(6) |

are consistent with the results of Pashov *et al.* [21] if one assumes for that work the same error bars of Ref. [16].

We also predict with high precision the value of the *s*-wave scattering length *a* for the absolute ground state; see Table IV. For two especially interesting pairs discussed in Ref. [16], the position of magnetic Feshbach resonances is recalculated with the current parameters [37]. Positions are slightly shifted with respect to the ones of [16] because of the different number of bound states in the singlet potential. They seem consistent with the plots shown in Ref. [18], which does not otherwise provide numerical values to compare with. We refer the reader to Ref. [16] for a discussion of possible applications of resonances in these specific K-Rb isotopic systems.

Finally, we present in Figs. 6 and 7 near-threshold-molecular potentials for the two pairs. One may note a level very close to dissociation associated with background scattering for both isotopic combinations, corresponding to a large positive $a_{bg}$. Avoided crossings of such a background level with magnetic-field-dependent molecular levels give rise to strong resonance shifts that can be given a simple analytic expression in terms of $a_{bg}$, $C_6$, and $\Delta$ [35]. For instance, the resonance at 39 G in Fig. 7 arises from the molecular level occurring at zero field near −0.25 GHz.

Again, using the parameters of Table IV one can see that both isotopic combinations present both broad open-channel-dominated resonances, which can be modeled theoretically by a single effective channel, and narrow closed-channel-dominated ones. The availability of such a broad range of properties should pave the way to the exploration of different quantum regimes in ultracold binary gases. Our data also provide a needed piece of information for the calculation of the Franck-Condon overlap matrix with electronically excited states and for implementing an efficient transfer scheme to low vibrational levels using Feshbach molecules as a bridge.

## IV. CONCLUSIONS AND OUTLOOK

In conclusion, we have performed extensive Feshbach spectroscopy of an ultracold $^{39}$K-$^{87}$Rb mixture. A combination of recent spectroscopic measurements on this system with data relative to the fermion-boson $^{40}$K-$^{87}$Rb system has allowed us to improve significantly the accuracy of our model. Interisotope analysis determines near-threshold parameters with better precision and fixes the number of bound levels supported by the interaction potentials. To the present level of precision no evidence for the breakdown of the Born-Oppenheimer approximation has been found. Therefore, we have determined by a straightforward mass scaling procedure different scattering properties for all K-Rb isotopic mixtures. The present results combined with information on short-range potentials is of crucial importance in order to determine the most convenient strategy for association of weakly bound molecules and their optical transfer into deeper bound states.

TABLE IV. Predicted zero-field *s*-wave scattering lengths *a* for the absolute ground state of K-Rb isotopes. Positions $B_{th}$, widths $\Delta_{th}$, background scattering lengths $a_{bg}$, and magnetic moments are also provided for Feshbach resonances of the two isotopic pairs of main experimental interest.

| K-Rb | $a$ $(a_0)$ | $B_{th}$ (G) | $\Delta_{th}$ (G) | $a_{bg}$ $(a_0)$ | $-s$ $(\mu_B)$ |
|---|---|---|---|---|---|
| 39–85 | 58.01(2) | | | | |
| 40–85 | −21.06(6) | | | | |
| 39–87 | 28.29(3) | | | | |
| 40–87 | −184.4(3) | | | | |
| 41–85 | 283.1(3) | 132.39(7) | 0.19 | 242 | 2.33 |
| | | 140.98(5) | 2.0 10$^{-4}$ | 242 | 3.42 |
| | | 146.4(3) | 0.025 | 242 | 2.88 |
| | | 185.2(9) | 3.5 | 327 | 2.14 |
| | | 191.72(7) | 0.48 | 327 | 2.14 |
| | | 672.19(15) | 5.7 | 343 | 1.89 |
| | | 695.90(12) | 14 | 343 | 1.70 |
| 41–87 | 640(3) | 39.4(2) | 37 | 284 | 1.65 |
| | | 78.92(9) | 1.2 | 284 | 1.59 |
| | | 558.0(4) | 81 | 173 | 1.14 |
| | | 724.8(3) | 0.07 | 90 | 1.93 |

[1] E. Tiesinga, B. J. Verhaar, and H. T. C. Stoof, Phys. Rev. A **47**, 4114 (1993).
[2] S. Inoyue, M. R. Andrews, J. Stenger, H.-J. Miesner, D. M. Stamper-Kurn, and W. Ketterle, Nature (London) **392**, 151 (1998).
[3] J. Stenger, S. Inouye, M. R. Andrews, H. J. Miesner, D. M. Stamper-Kurn, and W. Ketterle, Phys. Rev. Lett. **82**, 2422 (1999).
[4] T. Loftus, C. A. Regal, C. Ticknor, J. L. Bohn, and D. S. Jin, Phys. Rev. Lett. **88**, 173201 (2002).
[5] S. Inouye, J. Goldwin, M. L. Olsen, C. Ticknor, J. L. Bohn, and D. S. Jin, Phys. Rev. Lett. **93**, 183201 (2004).
[6] M. Zaccanti, C. D'Errico, F. Ferlaino, G. Roati, M. Inguscio, and G. Modugno, Phys. Rev. A **74**, 041605(R) (2006).
[7] S. Ospelkaus, C. Ospelkaus, L. Humbert, K. Sengstock, and K. Bongs, Phys. Rev. Lett. **97**, 120403 (2006).
[8] S. Jochim, M. Bartenstein, A. Altmeyer, G. Hendl, S. Riedl, C. Chin, J. Hecker Denschlag, and R. Grimm, Science **302**, 2101 (2003); M. Greiner, C. A. Regal, and D. S. Jin, Nature (London) **426**, 537 (2003); M. W. Zwierlein, C. A. Stan, C. H. Schunck, S. M. F. Raupach, S. Gupta, Z. Hadzibabic, and W. Ketterle, Phys. Rev. Lett. **91**, 250401 (2003).
[9] C. Ospelkaus, S. Ospelkaus, L. Humbert, P. Ernst, K. Sengstock, and K. Bongs, Phys. Rev. Lett. **97**, 120402 (2006); S. B. Papp and C. E. Wieman, *ibid.* **97**, 180404 (2006); J. J. Zirbel, K.-K. Ni, S. Ospelkaus, J. P. D'Incao, C. E. Wieman, J. Ye, and D. S. Jin, e-print arXiv:0710.2479; J. J. Zirbel, K.-K. Ni, S. Ospelkaus, T. L. Nicholson, M. L. Olsen, C. E. Wieman, J. Ye, D. S. Jin, and P. S. Julienne, e-print arXiv:0712.3889.
[10] A. Marte, T. Volz, J. Schuster, S. Durr, G. Rempe, E. G. M. van Kempen, and B. J. Verhaar, Phys. Rev. Lett. **89**, 283202 (2002).
[11] C. Chin, V. Vuletic, A. J. Kerman, and S. Chu, Phys. Rev. Lett. **85**, 2717 (2000).
[12] G. Modugno, G. Ferrari, G. Roati, R. J. Brecha, A. Simoni, and M. Inguscio, Science **294**, 1320 (2001).
[13] G. Roati, F. Riboli, G. Modugno, and M. Inguscio, Phys. Rev. Lett. **89**, 150403 (2002).
[14] G. Roati, M. Zaccanti, C. D'Errico, J. Catani, M. Modugno, A. Simoni, M. Inguscio, and G. Modugno, Phys. Rev. Lett. **99**, 010403 (2007).
[15] L. De Sarlo, P. Maioli, G. Barontini, J. Catani, F. Minardi, and M. Inguscio, Phys. Rev. A **75**, 022715 (2007).
[16] F. Ferlaino, C. D'Errico, G. Roati, M. Zaccanti, M. Inguscio, G. Modugno, and A. Simoni, Phys. Rev. A **73**, 040702(R) (2006).
[17] S. Inouye, J. Goldwin, M. L. Olsen, C. Ticknor, J. L. Bohn, and D. S. Jin, Phys. Rev. Lett. **93**, 183201 (2004).
[18] C. Klempt, T. Henninger, O. Topic, J. Will, W. Ertmer, E. Tiemann, and J. Arlt, Phys. Rev. A **76**, 020701(R) (2007).
[19] S. Kotochigova, P. S. Julienne, and E. Tiesinga, Phys. Rev. A **68**, 022501 (2003).
[20] D. Wang, J. Qi, M. F. Stone, O. Nikolayeva, H. Wang, B. Hattaway, S. D. Gensemer, P. L. Gould, E. E. Eyler, and W. C. Stwalley, Phys. Rev. Lett. **93**, 243005 (2004).
[21] A. Pashov, O. Docenko, M. Tamanis, R. Ferber, H. Knöckel, and E. Tiemann, Phys. Rev. A **76**, 022511 (2007).
[22] P. Soldán and V. Špirko, J. Chem. Phys. **127**, 121101 (2007).
[23] W. T. Zemke, R. Coté, and W. C. Stwalley, Phys. Rev. A **71**, 062706 (2005).
[24] J. P. D'Incao and B. D. Esry, Phys. Rev. Lett. **94**, 213201 (2005).
[25] C. Ticknor, C. A. Regal, D. S. Jin, and J. L. Bohn, Phys. Rev. A **69**, 042712 (2004).
[26] C. Amiot and J. Vergès, J. Chem. Phys. **112**, 7068 (2000).
[27] S. Rousseau, A. R. Allouche, and M. Aubert-Frécon, J. Mol. Spectrosc. **203**, 235 (2000).
[28] R. J. Le Roy, computer code RKR1 2.0, University of Waterloo, 2004.
[29] F. H. Mies, C. J. Williams, and P. S. Julienne, J. Res. Natl. Inst. Stand. Technol. **101**, 521 (1996).
[30] P. S. Julienne and S. Kotochikova (private communication).
[31] C. D'Errico, M. Zaccanti, M. Fattori, G. Roati, M. Inguscio, G. Modugno, and A. Simoni, New J. Phys. **9**, 223 (2007).
[32] A. Derevianko, J. F. Babb, and A. Dalgarno, Phys. Rev. A **63**, 052704 (2001).
[33] S. G. Porsev and A. Derevianko, J. Chem. Phys. **119**, 844 (2003).
[34] Bo Gao, E. Tiesinga, C. J. Williams, and P. S. Julienne, Phys. Rev. A **72**, 042719 (2005).
[35] K. Goral, T. Koehler, S. A. Gardiner, E. Tiesinga, and P. S. Julienne, J. Phys. B **37**, 3457 (2004).
[36] S. Falke, E. Tiemann, and C. Lisdat, e-print arXiv:0.706.2290.
[37] Recently, a few of the predicted features for the $^{41}$K-$^{87}$Rb isotopic pair have been experimentally observed at the predicted magnetic-field position: G. Thalhammer, G. Barontini, L. De Sarlo, J. Catani, F. Minardi, and M. Inguscio, e-print arXiv:0803.2763v1.